Applied Catalysis B: Environmental 256 (2019) 117791

Contents lists available at ScienceDirect

Applied Catalysis B: Environmental

journal homepage: www.elsevier.com/locate/apcatb

The effect of CO on CO_2 methanation over Ru/Al_2O_3 catalysts: a combined steady-state reactivity and transient DRIFT spectroscopy study

Leonardo Falbo[a], Carlo G. Visconti[a], Luca Lietti[a,*], János Szanyi[b,*]

[a] Department of Energy, Politecnico Di Milano, Milan, 20156, Italy
[b] Institute for Integrated Catalysis, Pacific Northwest National Laboratory, Richland, WA 99352, USA

ARTICLE INFO

Keywords:
Methanation
Power-to-gas
Ru/Al_2O_3 catalyst
Catalyst deactivation
DRIFTS-MS

ABSTRACT

The reactivity of Ru/Al_2O_3 catalysts in the hydrogenation of CO/CO_2 gas stream is investigated in this work to assess the possibility of carrying out CO_2 methanation even in the presence of CO in the feed stream. Such a goal is pursued by conducting reactivity studies at process conditions of industrial interest (i.e., at high CO_x per-pass conversion and with concentrated CO_x/H_2 streams) and by monitoring the surface species on the catalyst through transient DRIFTS-MS analysis. The catalyst shows gradual deactivation when the methanation is carried out in the presence of CO in the gas feed at low temperatures (200–300 °C). However, stable performance is observed at higher temperatures, showing CH_4 yields even higher than those observed during methanation of a pure CO_2 feed. DRIFTS-MS experiments agree with a CO_2 methanation pathway where CO_2 is adsorbed as bicarbonate on Al_2O_3 and successively hydrogenated to methane on Ru, passing through formate and carbonyl intermediates. In the presence of CO at low temperature, the catalyst shows a higher CO coverage of the Ru sites, a larger formate coverage of the alumina sites and the presence of adsorbed carbonaceous species, identified as carboxylate and hydrocarbon species. By carrying out the CO_2 hydrogenation on the deactivated catalyst, carboxylates remain on the surface, effectively blocking CO_2 adsorption sites. However, the catalyst deactivation at low temperature is reversible as thermal treatment (> 350 °C) is able to restore the catalytic activity. Notably, working above the carboxylate decomposition temperature ensures a clean catalyst surface without high CO coverage, resulting in stable and high performance in CO/CO_2 methanation.

1. Introduction

The growing atmospheric concentration of carbon dioxide is considered one of the main causes of global warming. Accordingly, during the last 20 years, several studies were carried out for intensifying the technologies aiming at its reduction [1–5]. Indeed, a drastic reduction of the CO_2 emissions to a near zero or even net-negative value is required by the end of the century to keep the temperature increase lower than 2 °C with respect to the pre-industrial levels (two-degree scenario or 2DS), which is considered a good compromise to avoid dangerous climate change [6,7]. According to this scenario, carbon capture and utilization (CCU) processes offer interesting perspectives. Among the suggested carbon dioxide re-utilization processes, the catalytic CO_2 hydrogenation to SNG (Synthetic or Substitute Natural Gas) is very attractive because it produces a fuel with a wide market and easily transportable with the existing infrastructures [8–11]. In addition, when using renewable H_2 produced by water electrolysis, SNG production from CO_2 hydrogenation represents a feasible route for the chemical storage of electric energy produced by renewable sources/nuclear plants. In fact, considering the fluctuating and intermittent nature of renewable energy sources (often collected in remote areas), an efficient way to store and to easily transport this energy is desirable, instead of being wasted [12–14]. This process of long-term storage, related to the use of CO_2 as carbon feedstock, is known as Power-to-Gas (PtG) technology [15].

The possibility of hydrogenating both carbon monoxide (Eq. (1)) and dioxide (Eq. (2)) to methane was discovered at the beginning of the 20th century by Paul Sabatier [16].

$$CO + 3\,H_2 \rightleftharpoons CH_4 + H_2O \quad \Delta H_R^0 = -206\,^{kJ}/_{mol}\ @298K \tag{1}$$

$$CO_2 + 4\,H_2 \rightleftharpoons CH_4 + 2\,H_2O \quad \Delta H_R^0 = -164\,^{kJ}/_{mol}\ @298K \tag{2}$$

Both reactions are strongly exothermic and bring to a molar contraction of the reacting mixture. Accordingly, low temperature and high pressure boost the carbon (both CO and CO_2) conversion, as reported in Figure S1 for different CO/CO_2 ratios in the gas feed. At suitable H_2/C

* Corresponding authors.
E-mail addresses: luca.lietti@polimi.it (L. Lietti), janos.szanyi@pnnl.gov (J. Szanyi).

https://doi.org/10.1016/j.apcatb.2019.117791
Received 13 December 2018; Received in revised form 26 May 2019; Accepted 28 May 2019
Available online 30 May 2019
0926-3373/

inlet ratio, thermodynamics allows the quantitative carbon conversion even at atmospheric pressure.

The methanation reaction is the process of choice for the purification of H_2 derived from syngas streams, but in this case the process operates with excess H_2 and diluted gas stream conditions. During the oil crisis in the late '70 s, methanation gained importance for the production of SNG by using syngas obtained from coal gasification as feedstock [8,17]. More recently, the increase in biomass utilization led to a renewed interest in the methanation reactions [12]. Regarding CO_2 methanation, the first pilot plant was built in the '90 s and nowadays the process is operated at commercial scale [11]. The typical feedstock is CO_2 obtained by separation from biogas or from the flue gases of power plants [14,18].

Both CO- and CO_2-methanation reactions (Eqs. (1) and (2)) are kinetically favored over VIII B group metal-based supported catalysts [19]. Due to their low price [12], nickel-based catalysts are the only ones used on industrial scale so far, although they are active in a temperature region where the conversion is limited by thermodynamics [19]. Furthermore, Ni-based catalysts are highly subjected to carbide [20] and policarbonyl [21] formation, resulting in deactivation by sintering [22] and volatilization [12,23], as well as to fouling phenomena [24] due to carbon whisker formation [20,25].

The most active metal for the methanation reactions is ruthenium [19,26], supported on different oxides such as Al_2O_3 [27,28], TiO_2 [29,30] and CeO_2 [31,32]. Ru-based catalysts are highly stable and selective in CO_2 hydrogenation, producing mostly CH_4 and only a small amount of CO as byproduct [33–36]. At the same time, they are also very active in CO hydrogenation [26], producing methane and some light hydrocarbons when working at low pressure and high H_2/CO molar ratio [37]. Furthermore, Ru-based catalysts are less prone to deactivation than the other methanation catalysts [10], even though some deactivation has been reported in the literature when working with gas feeds containing CO [38]. Sintering of small Ru-particles [39,40] and formation of volatile species as Ru-carbonyls [41] are reported among the possible causes of deactivation, although the most critical deactivation mechanism seems to be the formation and deposition of carbonaceous species, leading to active site blocking [42]. Carbon deposition is strongly affected by the process conditions [43,44] but does not lead to permanent deactivation, since high temperature treatments in hydrogen can restore the initial activity [45,46]. In any case, due to their high catalytic performance and long-term stability, Ru-based catalysts are attractive for process intensification in SNG production from both CO and CO_2.

The reaction pathways operating during both CO and CO_2 hydrogenation are still debated and depend on the nature of both the metal and the support, as well as on the process conditions [23,47,48]. On Ru-based catalysts, some authors propose that CO hydrogenation involves direct dissociation of chemisorbed CO (unassisted CO dissociation) [49–51], followed by a stepwise hydrogenation of adsorbed carbon to methane. At variance, other authors report that CO dissociation is assisted by chemisorbed hydrogen on a near-by site (H-assisted CO dissociation) [47,51–53], leading to the formation of an oxygenated intermediate. Concerning CO_2 methanation, most studies agree that CO is a reaction intermediate [30,54–58]. The CO formation mechanism, however, is debated as well. It has been suggested that CO is produced through the reverse water gas shift reaction, where the CO_2 is first adsorbed on the support surface as bicarbonate and then transformed into formate species, which is the precursor of adsorbed CO on the Ru sites [57,58]. As alternative route, other authors suggest that CO_2 is adsorbed dissociatively on the Ru sites, producing CO and O, with the formation of some spectator species (i.e., formates) [53]. Eventually, CO is hydrogenated to CH_4, according to H-assisted [51,58] or unassisted [59] pathways.

On these bases, the purpose of this work is to deepen the mechanistic understanding related to the CO_2 methanation reaction over Ru-based catalysts, with particular emphasis on the role of CO. Accordingly, the hydrogenation of CO_2, CO and CO/CO_2 mixtures has been investigated. A 0.5 wt.% Ru/Al_2O_3 catalyst has been considered in this study and tested in a fixed bed reactor at process conditions relevant to the industrial scale SNG production. The reactivity study has been accompanied by a detailed characterization of the surface species involved in both CO_2 and CO hydrogenation by using in situ diffuse reflectance infrared Fourier-transform spectroscopy (DRIFTS).

2. Experimental

2.1. Catalysts

The catalyst used for the activity tests in the fixed bed reactor was a commercial 0.5 wt.% Ru/Al_2O_3 sample (Aldrich, 206199). This sample, which is referred to as Ru-SA, came in the form of cylindrical pellets (d_p = 3.2 mm, h_p = 3.6 mm), with eggshell geometry. The SEM-EDX analysis of an axially cut catalyst pellet showed an amount of ruthenium in the external shell (thickness of 210 ± 20 μm) equal to 4.5 wt. % [33].

In situ experiments in the DRIFTS cell were carried out with a reference in-house prepared catalyst, obtained by homogenous impregnation of an alumina support [35]. Specifically, a γ-Al_2O_3 powder (Sasol Puralox SCCa 150/200) was impregnated with an aqueous ruthenium nitrosyl nitrate solution (Aldrich, 373567) in order to obtain a nominal metal loading of 5 wt.%, a value close to the Ru amount in the commercial catalyst's shell. A 30% excess of the impregnating aqueous solution with respect to the alumina pore volume was used. After impregnation, the sample was dried in static air at 100 °C overnight. This sample, referred to as Ru-N, showed comparable reactivity with respect to the commercial Ru-SA sample.

2.2. Catalyst characterization

Textural properties of the samples were determined by N_2 adsorption-desorption isotherms, measured at 77 K by using a Micromeritics Tristar 3000 instrument. Prior to the analysis, each sample was powdered and evacuated at 100 °C for 3 h.

Transmission electron microscopy (TEM) imaging was performed on the in-house prepared catalyst (Ru-N) with a high-resolution microscope (FEI Titan 80-300) operated at 300 kV, equipped with a CEOS GmbH double-hexapole aberration corrector for the probe-forming lens, allowing imaging with 0.1 nm resolution.

The ruthenium loading of the in-house prepared supported catalyst (Ru-N) was determined by inductively coupled plasma (ICP) mass spectrometry (Thermo Electron, X series 2 ICP-MS) on the mineralized sample, successively diluted with nitric acid. The same treatment was not applicable to the commercial catalyst (Ru-SA), which was not fully dissolved in the acid treatment.

Metal dispersion on the support was calculated by H_2 chemisorption analyses performed by a Micromeritics AutoChem II instrument. The powdered catalyst (0.1 g) was loaded into a quartz reactor and activated at 400 °C for 3 h (2 °C/min) in a 10 vol.% H_2/Ar gas mixture at 18 L(STP)/h/g_{cat}. After activation, the sample was purged in He at 400 °C for 2 h, cooled to room temperature and successively heated at 100 °C. Pulses of diluted H_2 (10 vol.% H_2/Ar) were added at 100 °C and the metal dispersion was estimated based on the molar ratio of adsorbed H_2 and the overall Ru loading, considering a Ru:H_2 = 2:1 ratio.

2.3. Activity tests in the macro reactor

Activity tests were carried out in a lab-scale rig operating 24/7 and described elsewhere in detail [33]. Briefly, the unit was equipped with a fixed-bed reactor (internal diameter 1.1 cm, length 23 cm), placed into an electric tubular furnace. The feed gases, whose flow rate was controlled by electronic mass-flow meters (Brooks Instruments), were sent to the reactor. The unconverted gases and the reaction products

leaving the reactor were sent to a cold trap (T = 0 °C) in order to condense produced water. Reactants and products were analyzed by using an on-line gas chromatograph (Agilent, 6890) equipped with two wide-bore columns each connected to a thermal conductivity detector (TCD) used to quantify the concentrations of H_2, Ar, N_2, CH_4, CO, CO_2 and C_2-C_5 hydrocarbons. C_{3+} hydrocarbons and oxygenated species were never detected during either CO or CO_2 hydrogenation. Traces of ethane were detected only in the presence of CO in the gas feed, however, its selectivity never exceeded 1% of the total carbon converted. Carbon balances, defined as ratio of the total amount of carbon in the products and the converted carbon, always closed within ± 5%.

In a typical run, 0.375 g of Ru-SA catalyst, crushed and sieved below 106 μm, were loaded into the reactor diluted with inert α-Al_2O_3 (volumetric dilution ratio equal to 1). The absence of intra- and inter-porous mass transfer limitations was checked both theoretically and experimentally [33]. Prior to each run, the catalyst was activated by in situ reduction at 400 °C (heating rate: 2 °C/min) for 3 h in pure hydrogen with a space velocity of 1.8 L(STP)/h/g_{cat} and atmospheric pressure. Thereafter the reactor was cooled down to 250 °C in N_2 flow (5 L(STP)/h/g_{cat}) and eventually slowly heated at 350 °C (heating rate: 1 °C/min) while the N_2 flow was progressively replaced by the reactant stream. The achieved process conditions (T = 350 °C, GHSV = 5 L(STP)/h/g_{cat}, P = 1 ata, H_2/CO_2 = 4 mol_{H2}/mol_{CO2}) were then kept until steady CO_2 conversion was attained.

The role of CO on the catalyst activity was investigated at T = 310 °C, GHSV = 5 L(STP)/h/g_{cat}, P = 1 ata, H_2/C = 4 mol_{H2}/mol_C and P^0_{Ar} = 0.01 ata, while changing the CO/CO_2 inlet ratio in the range 0–4 mol/mol (Table 1). Reference process conditions were set at CO/CO_2 = 0 in Table 1 ("CO free" conditions). The effect of temperature (in the range 290–400 °C) was also investigated, while keeping constant all other process conditions (GHSV = 5 L(STP)/h/g_{cat}, P = 1 ata, H_2/C = 4 mol_{H2}/mol_C and P^0_{Ar} = 0.01 ata). The reactivity of the catalyst in each run was monitored for 2 h. Long-term stability of the catalyst was also studied, starting with the fresh catalyst.

The stability of the catalyst was evaluated by monitoring the conversion and selectivity trends with time-on-stream (T.o.S), before and after the CO co-feeding. Carbon conversion (χ_C) was calculated by using the following Eq. (3):

$$\chi_C = \frac{F^{IN}_{CO_2} + F^{IN}_{CO} - F^{OUT}_{CO_2} - F^{OUT}_{CO}}{F^{IN}_{CO_2} + F^{IN}_{CO}} \quad (3)$$

In Eq. (3) $F^{IN}_{CO_2}$ and F^{IN}_{CO} are the inlet molar flowrates, while $F^{OUT}_{CO_2}$ and F^{OUT}_{CO} are the molar flowrates leaving the reactor, for the species CO_2 and CO, respectively.

2.4. In situ transient DRIFTS-MS measurements

The in situ infrared spectra were collected by using a FT-IR spectrometer (ThermoFisher Nicolet iS 50R FT-IR), fitted with a liquid-N_2 cooled MCT detector and equipped with DRIFTS accessories and a high-temperature cell (Harrick, HVC-DRP). Each IR spectrum was recorded at 4 cm^{-1} resolution and was the average of 32 scans. Collected DRIFT spectra are reported in this work as absorbance, which can be considered almost proportional to the concentration of adsorbed species on the catalyst surface [60]. The evolution of adsorbed surface species amount during the time on stream was calculated by integrating the intensity of peaks univocally related to an adsorbed species, by using end-points straight line as baseline.

The DRIFTS reactor cell was calibrated for a correct temperature measurement in the catalytic bed region radiated by the IR beam [61]. Two gas feeding manifolds, equipped with mass flow controllers and connected to a 4-way valve, were used to introduce gases into the reactor cell with desired flowrate and composition. The gas leaving the cell was analyzed by a mass spectrometer (UTI 100C). The following mass-to-charge ratios (*m/z*) were used to follow the concentration of the various species: 2 (H_2), 15 (CH_4), 18 (H_2O), 28 (CO + contribution due to CO_2 fragmentation) and 44 (CO_2).

During the DRIFTS experiments, the undiluted Ru-N catalyst sample was placed into the reactor cell (catalyst weight around 80 mg). After activation at 350 °C for 3 h in flowing H_2 (2.4 mL/min), the catalyst was cooled down to 200 °C and purged in He for 2 h. Then H_2/He = 8/92, H_2/CO_2/He = 8/2/90, H_2/CO_2/He = 5/5/90, H_2/CO/He = 8/2/90 or H_2/CO/CO_2/He = 8/1.6/0.4/90 (molar ratios) mixtures were fed with a flowrate of 15 mL/min, and both the gas and the surface phase were monitored. Before each experiment, the activation procedure was repeated and then a background IR spectrum in He was taken at the investigated temperature.

Table 1
Gas feed compositions during the CO_x hydrogenation in the fixed bed reactor (T = 310 °C, P = 1 ata, GHSV = 5 L(STP)/h/g_{cat}, catalyst Ru-SA).

$\frac{CO}{CO_2}\left[\frac{mol}{mol}\right]$	0	0.25	0.5	0.75	1	2	4
$\frac{CO}{CO+CO_2}\left[\frac{mol}{mol}\right]$	0	0.20	0.33	0.43	0.50	0.67	0.80
P^0_{CO} [ata]	0	0.04	0.07	0.09	0.10	0.13	0.16
$P^0_{CO_2}$ [ata]	0.20	0.16	0.13	0.11	0.10	0.07	0.04
$P^0_{H_2}$ [ata]	0.79	0.79	0.79	0.79	0.79	0.79	0.79
P^0_{Ar} [ata]	0.01	0.01	0.01	0.01	0.01	0.01	0.01

3. Results and discussion

3.1. Catalyst characterizations

The commercial Ru-SA catalyst has an egg-shell geometry and a Ru loading in the egg-shell layer equal to 4.5 wt.%, measured by SEM-EDX (Table 2). The BET surface area of the powdered sample is 103 m^2/g, and the overall Ru dispersion is 35%.

The in-house prepared Ru-N catalyst has a surface area of 175 m^2/g, close to that of the alumina support (200 m^2/g), and higher than that of the commercial material. The ruthenium loading (measured by ICP) is 4.4 wt.%, while the Ru-dispersion is 31%. These values are comparable to those of the eggshell Ru-SA catalyst. The micrographs of the fresh Ru-N catalyst (Figure S2) show Ru particle sizes lower than 1 nm, with a particle size distribution centered in the 6–8 Å range.

3.2. Macro reactor experiments

As we have reported it previously [33], the Ru-SA catalyst exhibits stable performance during CO_2 methanation, with high CO_2 conversion and high carbon selectivity to methane (higher than 99% at process conditions relevant for industrial scale operations, with CO being the only byproduct). The same catalyst was tested in CO/CO_2 hydrogenation, keeping constant the H_2/C inlet molar ratio. The first set of CO/CO_2 co-feeding experiments was carried out at 310 °C by varying the CO/CO_2 ratio in the gas feed (Table 1). Fig. 1 shows the CO_2, CO and overall C conversions as a function of time on stream (T.o.S.) for different values of the CO/CO_2 ratio.

Under "CO free" conditions (CO/CO_2 = 0, T.o.S. = 143–145 h in Fig. 1) the catalyst shows a stable CO_2 conversion value of 58% with a

Table 2
Textural and morphological properties (Metal loading: * SEM/EDX, X declared by producer, + ICP).

	BET surface area [m^2/g]	Metal loading [wt.%]	Metal dispersion [%]
Ru-SA	103	4.5 (shell) * 0.5 (overall) X	35
Ru-N	175	4.4 +	31

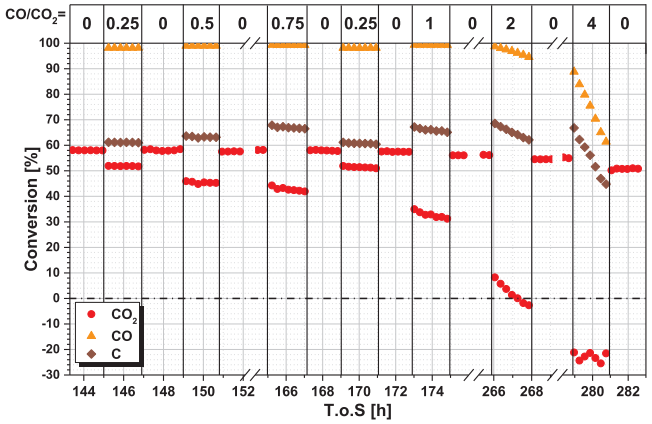

Fig. 1. Evolution with T.o.S. of CO_2, CO and CO + CO_2 (C) conversions during CO_x hydrogenation at different CO/CO_2 inlet molar ratios [Process conditions: T = 310 °C, P = 1 ata, GHSV = 5 L(STP)/h/g_{cat}, H_2/C = 4 mol_{H2}/mol_C, P^0_{Ar} = 0.01 ata, catalyst: Ru-SA].

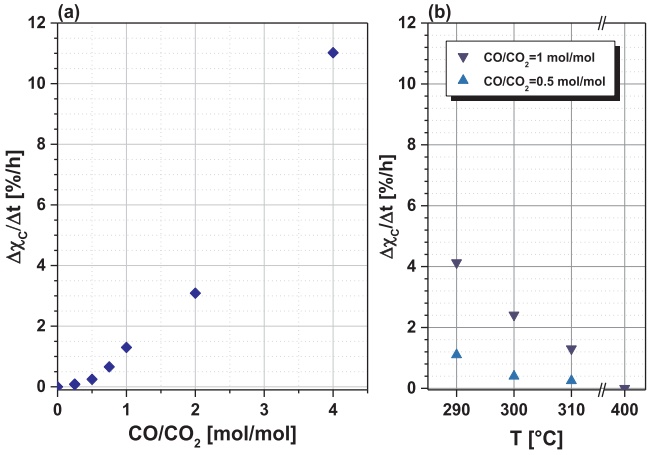

Fig. 2. Activity loss as function of (a) the CO/CO_2 inlet ratio at T = 310 °C and (b) the temperature at CO/CO_2 inlet ratio equal to 0.5 and 1 mol_{CO}/mol_{CO2} [Other process conditions as Fig. 1].

99.5% selectivity to methane. When CO is added to the gas phase (CO/CO_2 molar ratio of 0.25, T.o.S. = 145–147 h) the CO_2 conversion drops to a value of 52%, while the co-fed CO is quantitatively converted. This brings to an overall C conversion higher than that measured under "CO free" conditions, very likely due to the increase of the H_2/CO_x stoichiometric value. Notably, the observed decrease in the CO_2 conversion is not due to a kinetic effect resulting from the decrease of P_{CO2}, as shown in a previous kinetic study [33]. During the CO co-feeding, the process produces mainly CH_4 and only traces of ethane are detected.

Experimental data indicate an inhibiting effect of CO on the CO_2 conversion, although the overall CH_4 production is increased. This is in line with a scheme of consecutive reactions for the CO_2 methanation reaction, being adsorbed CO the intermediate in CH_4 formation [55]. CO admission inhibits CO_2 adsorption (thus decreasing CO_2 conversion), but pushes CH_4 formation due to CO hydrogenation. Notably, during the CO/CO_2 = 0.25 co-feeding period, the CO_2 conversion slightly decreases with T.o.S., showing a loss of 0.2% in 2 h on stream, while the CO conversion remains almost complete during the whole period. Returning to the "CO free" process conditions, the catalyst activity in the CO_2 hydrogenation is almost completely recovered. The process conditions with a CO/CO_2 inlet ratio of 0.25 were tested twice in order to evaluate reproducibility, which was fully confirmed (T.o.S. = 169–171 h in Fig. 1).

By further increasing the CO/CO_2 inlet ratio to values of 0.5 and 0.75, the observed effects (both in terms of decrease in the CO_2 conversion and deactivation) become more pronounced; at CO/CO_2 inlet ratio equal to 1 (T.o.S. = 173–175 h), besides the activity loss during the cofeeding period, the catalyst shows also an appreciable permanent deactivation when the "CO free" process conditions are restored, at T.o.S. = 175 h. By further increasing the CO/CO_2 ratio to a value of 2 (T.o.S. = 266 h), the CO_2 methanation inhibition due to the presence of CO in the gas feed is very strong so that CO_2 conversion suddenly drops below 10%, while the CO conversion remains complete. Under these conditions, however, the catalyst is rapidly deactivated so that the CO_2 conversion at first goes to zero and then becomes even negative (i.e. CO_2 becomes a reaction product). Methanation with a CO/CO_2 = 2 gas mixture results in a more severe catalyst deactivation and, consequently, the measured CO_2 conversion value after the CO co-feeding (T.o.S. = 268 h) is lower than the value measured before (T.o.S. = 265 h).

Deactivation effects are further amplified by working with a CO/CO_2 inlet ratio equal to 4 (T.o.S. = 279–281 h). As a matter of facts, the deactivation rate, calculated as loss of carbon conversion per time unit (Fig. 2(a)) rises more than linearly with the concentration of CO in the gas feed stream.

These results are in agreement with those described by Ekerdt and Bell [46], who reported the deactivation of Ru-based catalysts when working with H_2/CO mixtures. They showed that the deactivation rate increases with the CO partial pressure, due to an inhibition of CO on H_2 adsorption. Similar effects were also observed by other authors [42,62], although the reason for deactivation was not clearly explained. Bell et al. [63] proposed that carbon deposition was the main reason for the catalyst deactivation, while Gupta et al. [64] proposed that the formation of di- and tri-carbonyls, more difficult to hydrogenate, is responsible for the deactivation during CO hydrogenation.

To better investigate the deactivation phenomena, a second set of CO/CO_2 co-feeding experiment was carried out by varying the temperature in the range of 290–400 °C at different CO/CO_2 inlet ratios. The results, displayed in Figure S3 in the supplemental material, showed that the effect of CO addition is more evident at low temperature: the 2h-average deactivation rate observed during the CO/CO_2 co-feeding, showed in Fig. 2(b), increases with decreasing temperature.

3.3. *In situ DRIFTS-MS measurements*

In order to identify the key surface species during the methanation of CO_2, CO and CO/CO_2 mixtures, in situ DRIFTS-MS measurements were carried out at 200 °C using the homogenously impregnated in-house prepared catalyst (Ru-N). Catalyst performance into fixed bed reactor configuration can be found elsewhere [35]. The temperature was reduced with respect to the experiments reported in Section 3.2, with the purpose of favoring the deactivation phenomena during the CO feed.

3.3.1. *CO_2 hydrogenation*

Fig. 3(a) shows MS signals for the species leaving the DRIFT cell in the gas phase during CO_2 hydrogenation. At T.o.S. = 0 h CO_2 and H_2 were admitted to the reactor; the methane concentration shows a maximum at 5 min on stream, and then reaches a steady state value after 20 min. Evolution of the m/z = 28 signal is also observed, but this mostly results from the contribution of CO_2 fragmentation in the mass spectrometer.

The corresponding recorded DRIFT spectra are shown in Fig. 3(b). The observed IR bands are related to species in gas phase, as well as adsorbed on both the Al_2O_3 support and the Ru particles. Specifically, IR features of gas phase CO_2 are centered at 2349 cm^{-1}, while the produced gas phase CH_4 shows the typical δ_{CH} bending vibrational feature at 1305 cm^{-1} and the asymmetric $\nu_{C\text{-}H}$ stretching vibration at 3016 cm^{-1} (see inset). The rotational vibrational spectrum of gaseous water, the main byproduct of the Sabatier reaction, is observed in the

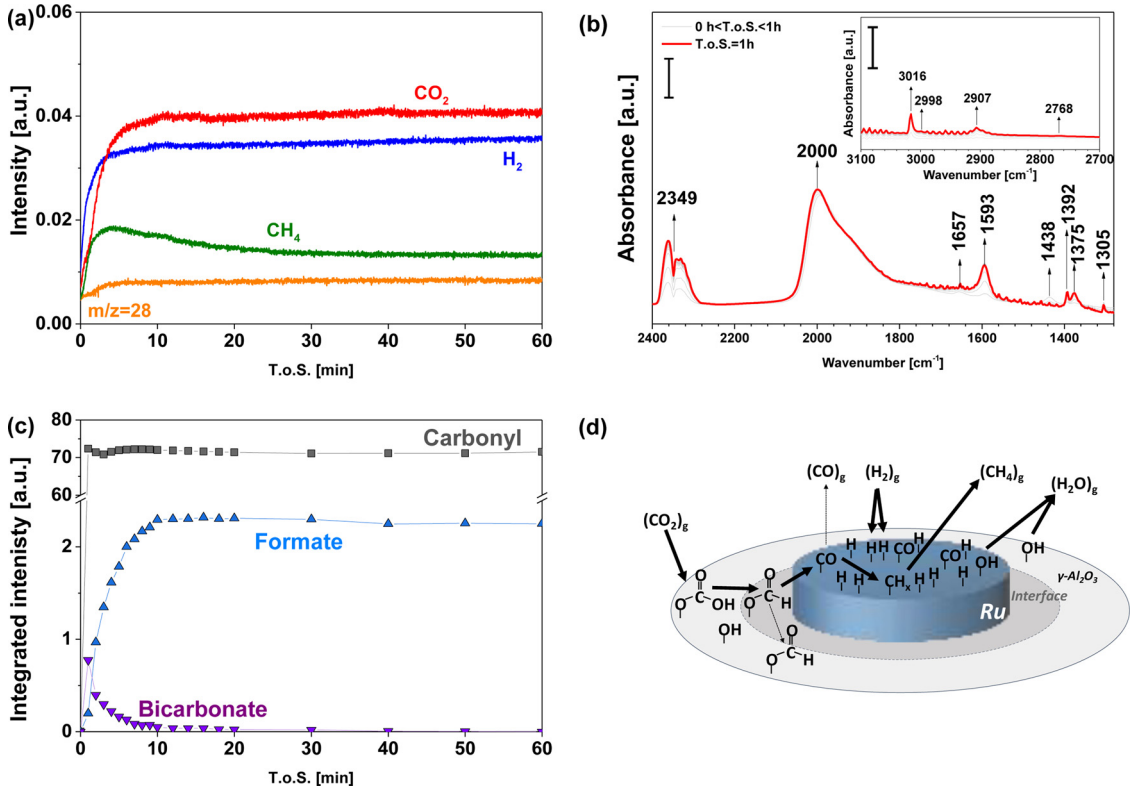

Fig. 3. CO_2 methanation at 200 °C: (a) MS signals for the gas phase as function of the T.o.S, (b) DRIFT spectra (inset 3100-2700 cm^{-1} wavenumber region), (c) corresponding intensity trends for the adsorbed species and (d) schematic representation of reaction pathway (solid arrows show the main paths). [Process conditions: T = 200 °C, P = 1 ata, F = 15 mL/min, $H_2/CO_2/He$ = 8/2/90 M ratios, catalyst: Ru-N].

1800 ÷ 1300 cm^{-1} range.

Focusing on the species adsorbed on the catalyst surface, the IR bands at 1657 and 1438 cm^{-1} represent the asymmetric and symmetric OCO-stretching vibrations of the adsorbed bicarbonate species (in addition to the OH deformation at 1228 cm^{-1}, not shown), formed upon reaction between CO_2 and the hydroxyl groups of the Al_2O_3 support [34,65–68]. Furthermore, formate species are also detected, with bands at 1593, 1392 and 1375 cm^{-1} associated with the asymmetric OCO-stretching, CH-deformation and symmetric OCO-stretching, respectively [45,58,69]. Additionally, the formates show a high wavenumber vibration at 2907 cm^{-1}, associated with the CH-stretching, and two peaks at 2998 and 2768 cm^{-1}, related to the combination of vibrations previously described [69]. The complex peak in the range 2080 ÷ 1800 cm^{-1}, with the maximum at ~2000 cm^{-1}, is assigned to carbonyls on the Ru-surface in multiple bonding configurations [30,46,58,70–72]. Indeed, the shape and the lower wavenumber tail of this peak indicate that CO is not present only in the linear configuration on the metallic Ru, but also in the bridging and three-folded configuration on different coordination Ru sites.

The evolution of the detected species on the catalyst surface as function of T.o.S. is reported in terms of integrated band intensities in Fig. 3(c) (bicarbonate = 1438 cm^{-1}, formate = 1392 + 1375 cm^{-1}, carbonyl = 2080 ÷ 1800 cm^{-1}). The bicarbonate concentration shows a maximum and then decreases to a very small steady state value. At variance, the concentration of formate species monotonically increases with time on stream and reaches a steady state value. The broad band representing adsorbed CO reaches its maximum almost instantaneously and retains its value during the entire analysis time. These trends are in line with prior literature [57,58], sketched in Fig. 3(d) and further highlighted below:

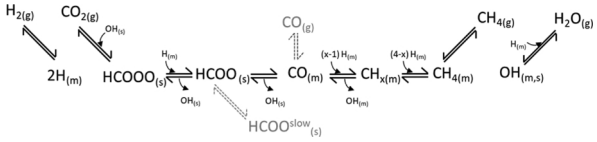

where (m) is a metal site and (s) is the support. Briefly, CO_2 is adsorbed on the catalyst support forming bicarbonate species, which are hydrogenated to formates at the metal-support interface by hydrogen dissociatively adsorbed on the metal sites. The formates can be further hydrogenated producing CO adsorbed on the Ru sites or migrate and accumulates on the alumina support. The adsorbed CO is then stepwise hydrogenated to methane rather than released in the gas phase, as suggested by the low CO selectivity.

3.3.2. CO hydrogenation

The results obtained during the CO hydrogenation over the Ru-N catalyst sample are shown in Fig. 4. In this case the dynamics is slower than that of CO_2 and therefore, to better understand the phenomena occurring on the catalyst surface, the length of the experiments was increased to 24 h.

Fig. 4(a) shows the MS signals of the species exiting the DRIFTS cell during the first hour on stream, which describes the observed initial transient. The gas phase CH_4 signal shows a maximum after a few minutes and then progressively decreases with time on stream. The deactivation continues during the whole experiment period as pointed out by the trace of integrated intensity of gas phase methane (peak at 3016 cm^{-1}) showed in Fig. 4(c).

The DRIFT spectra recorded during CO hydrogenation (Fig. 4(b)) show significant differences with respect to those recorded during CO_2 hydrogenation (Fig. 3(b)). The gas phase CO bands, centered at 2143 cm^{-1}, are visible along with only very little amounts of gas phase CO_2 produced by the reaction, as further confirmed by MS signals.

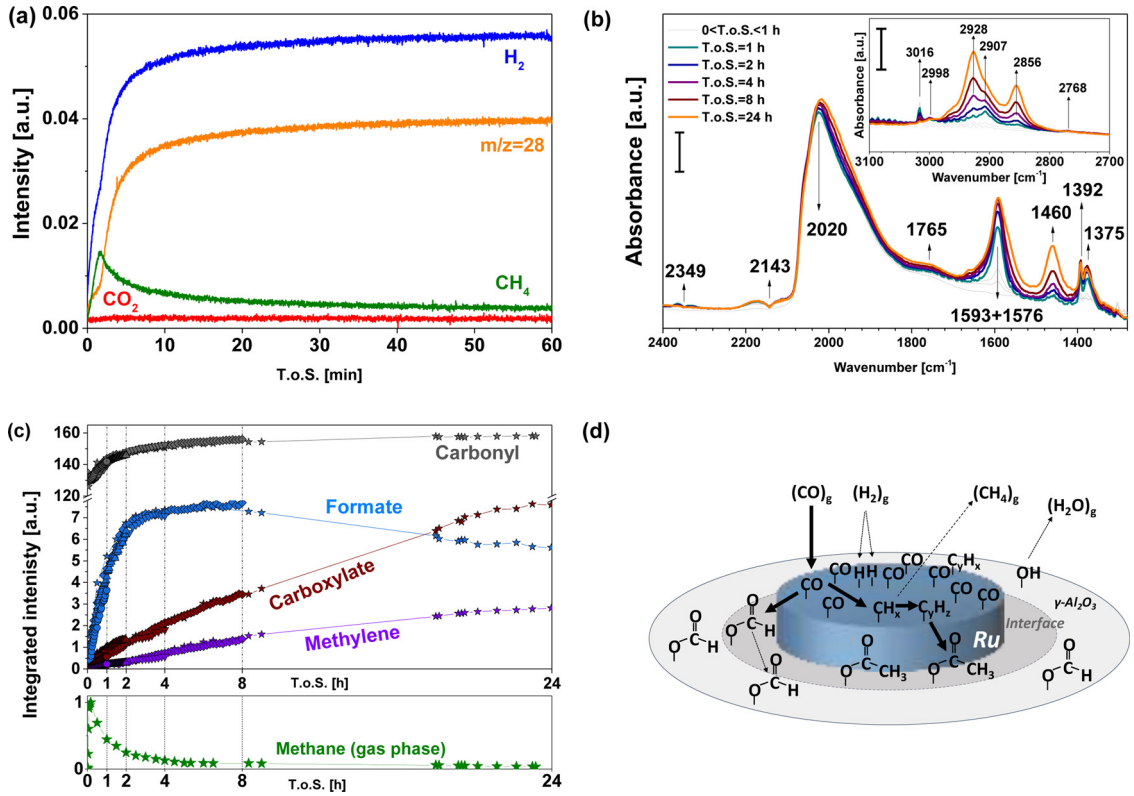

Fig. 4. CO methanation at 200 °C: (a) MS signals for the gas phase as function of the T.o.S, (b) DRIFT spectra (inset 3100-2700 cm^{-1} wavenumber region), (c) corresponding intensity trends for the adsorbed species and gas phase methane, (d) schematic representation of reaction pathway (solid arrows show the main paths). [Process conditions: T = 200 °C, P = 1 ata, F = 15 mL/min, H_2/CO/He = 8/2/90 M ratios, catalyst: Ru-N].

Looking at the adsorbed surface species, bicarbonates are not observed during the CO hydrogenation, while formates are much more abundant on the catalyst surface than on the CO_2/H_2 gas stream (Fig. 3(b)). Also, a new peak located at 1460 cm^{-1} appears, which has been attributed to the symmetric OCO-stretching of carboxylate groups (e.g. acetates) [38,73,74]. The asymmetric OCO-stretching vibration of this species is located at ~1576 cm^{-1}, but it is masked by the feature of the formate species at 1593 cm^{-1}. Literature reports the formation of carboxylates on alumina support by interaction of hydrocarbons with the alumina hydroxyl groups [74,75]. Furthermore, in analogy to what reported in the Fischer-Tropsch literature, although working at different process conditions, carboxylate species could also be formed on the metal by insertion of CO during the hydrocarbon chain growth [76]. Nevertheless, on the basis the adsorption of acetic acid on Ru(0001) [77], it is likely that the carboxylates are adsorbed, at least partially, on the alumina.

The intensity of the carbonyl related bands in the range 2080 ÷ 1800 cm^{-1} is strongly enhanced with respect the case of CO_2 hydrogenation, suggesting that the CO coverage on ruthenium is enhanced by the presence of CO in the feed stream. The appearance of the broad and weak band around 1765 cm^{-1} suggests the formation of bridged carbonyls, even though we cannot exclude that this band is due to another type of surface species [78]. In any case, in the following we will refer to a unique CO adsorbed species even if we do expect a different reactivity of the different CO adsorbed species.

Two bands, not visible during CO_2 hydrogenation, are also detected in the CH-stretching region during CO hydrogenation, in addition to those associated with formates and gas phase CH_4. They are centered at 2928 and 2856 cm^{-1} and are both related to the stretching vibrations of methylene groups, indicating the presence of methylene fragments (Ru = CH_2) and/or aliphatic hydrocarbons on the catalyst surface [38,73], most probably on the Ru particles [46,79], even if some authors proposed the same features for hydrocarbons adsorbed on the alumina surface [45]. Furthermore, because of the interference with the vibrational peaks of the gas phase methane, for short time on stream it is not possible to observe another band at 2966 cm^{-1} related to the methyl group [46,79], but it is clearly observable at T.o.S. = 24 h.

The integrated intensities of the IR bands observed during CO hydrogenation are shown in Fig. 4(c) as a function of time on stream. The intensity of the multi-bonded carbonyl peak rapidly increases with T.o.S., especially during the first 2 h on stream. This seems to be related with the observed deactivation rate in CH_4 formation as observed in the MS signal (Fig. 4(a) and (c)). This behavior indicates that the coverage of the active sites by CO increases during CO hydrogenation, progressively decreasing the number of active sites available for the dissociative H_2 adsorption. It is speculated that this is one of the causes of the deactivation phenomena observed during the CO hydrogenation [80], and is also in line with the observed kinetics of the CO methanation showing positive order with respect the H_2 and negative order with respect the CO [37,43]. This also well explains the reactivity behavior of the Ru-SA catalyst (Fig. 2) which undergoes deactivation at low temperature and high CO/CO_2 ratio in the gas feed, conditions that decrease the H/CO ratio on the catalyst surface.

Besides carbonyls, the formate surface concentration increases during the first 2 h on stream, reaching a maximum around 6–8 h, with an amount about three times higher than that observed during CO_2 hydrogenation. Then the concentration of formates slightly decreases with time on stream. Dalla Betta and Shelef [45], based on their isotopic exchange experiments, reported that the formate species are not reaction intermediates, but byproducts adsorbed on the alumina support (spectator species). It is worth to note that the behavior and role of formate species during CO hydrogenation is different from that observed in CO_2 methanation, where they act as precursors of CO formation. Notably, Dalla Betta and Shelef [45] reported that formates can be formed directly on the alumina surface from the reaction of H_2 and CO even in the absence of metallic Ru. Besides, as suggested by Lorito

et al. [73] for a similar catalyst, an additional route for formate production is the spillover of CO from the metallic Ru sites to the alumina support. Accordingly in the case of CO hydrogenation it is speculated that the concentration of formates initially increases with time-on-stream due to the saturation coverage of the alumina support, and then slightly decreases being involved in the formation of other species bonded to the alumina surface (e.g., CH_x-containing surface species).

Fig. 4(c) also shows that the surface coverage of methylene species (calculated by integrating the 2856 cm^{-1} band) linearly increases with the time on stream. Since no decrease in the CO coverage was observed during the accumulation of these species, they are likely located only on a small portion of the metal surface. During the experiments no hydrocarbons other than CH_4 were detected by MS in the gas phase. This indicates that their concentration is too low to be detected and/or that, if produced, they remain adsorbed on the catalyst surface. Eventually, the carboxylate species (whose trend was calculated by integrating the 1460 cm^{-1} band) show a continuous concentration increase, reaching a near saturation value after 24 h on stream.

Based on these evidences, the following pathways can be envisaged for CO hydrogenation, also depicted in Fig. 4(d):

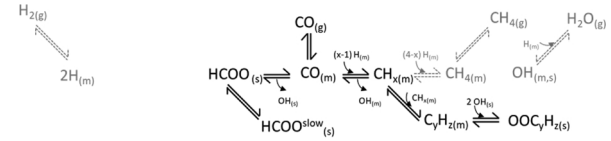

CO is initially strongly adsorbed on Ru sites, progressively reducing the active sites for the hydrogen dissociative adsorption. The adsorbed CO can be hydrogenated on metallic Ru to CH_x species (leading to methane) and other carbonaceous species, which remain adsorbed on Ru. The reaction of CO with surface hydroxyls may also lead to formate species at the Ru/Al_2O_3 interface that can spill over the alumina support. Carboxylate species can also be formed, upon reaction of hydrocarbons with alumina hydroxyls groups: these species likely remain adsorbed at the Ru/Al_2O_3 interface. Finally, small amounts of gas phase CO_2 are also produced, due to the occurrence of the water gas shift reaction.

Notably, formation of CH_4 and other hydrocarbons from CO implies the breaking of the C–O bond. As discussed above, this may occur according to a direct CO dissociation pathway leading to C- and O-ad-species, or, more likely, through an H-assisted CO dissociation pathway [47,51–53]:

$$CO_{(m)} + H_{(m)} \rightarrow HCO_{(m)} + *_{(m)}$$

$$HCO_{(m)} + x\ H_{(m)} \rightarrow CH_{x(m)} + OH_{(m)}$$

3.3.3. CO/CO_2 hydrogenation

Finally, DRIFTS-MS experiments were performed during the CO/CO_2 methanation. As shown in Fig. 5(a), in these experiments the reactivity of CO_2/H_2 was initially investigated (T.o.S. = 0–20 min) and then, after a He purge, the feed was switched to $CO/CO_2/H_2$ (T.o.S. = 30–70 min). Eventually, the reactivity of CO_2/H_2 was investigated again (T.o.S. = 80–100 min).

The DRIFT spectra of the surface, recorded at relevant T.o.S. (20, 70 and 100 min), i.e. at the end of each different feed, are shown in Fig. 5(b), while Figure S4 provides the complete series of IR spectra collected during the whole experiment.

Spectrum 1 of Fig. 5(b) shows the species during CO_2 hydrogenation, and accordingly multi-bonded CO and formates are adsorbed on the catalyst surface, as previously discussed. By introducing CO into the gas feed (T.o.S. = 30–80 min) the catalyst is deactivated, as shown by the MS signal of CH_4 in Fig. 5(a). At the end of this period (spectrum 2 in Fig. 5(b), T.o.S. = 70 min), the concentration of the adsorbed CO is greatly increased, reaching an intensity similar to the case of pure CO hydrogenation (Fig. 4(b)). Furthermore, during this period, the formate intensity is also increased and IR bands characteristic of hydrocarbons and carboxylates appear (inset of Fig. 5(b)). As a matter of facts, the behavior of the catalyst during CO/CO_2 hydrogenation is similar to that observed during hydrogenation of pure CO and described in Fig. 4.

By returning to CO_2 hydrogenation process conditions (T.o.S. = 80–100 min), the catalyst shows a loss of activity as pointed out by the MS signals of CH_4 and CO_2. The corresponding IR spectrum (spectrum 3 in Fig. 5(b)) shows that the CO band decreases back to the intensity of spectrum 1, and the bands of methylene groups cannot be observed. In contrast, the formate and carboxylate peaks retain their intensities during the whole period. Accordingly, the main differences between the surface observed during CO_2 hydrogenation on fresh catalyst and the deactivated one (i.e. after CO/CO_2 hydrogenation) are the presence, in the latter case, of the bands of carboxylate species (inset-Figure 5(b)) and a slightly higher CO coverage.

The same set of experiments has been repeated at a higher temperature, 250 °C, and results are shown in Fig. 6(a) (MS signal intensities) and Fig. 6(b) (representative IR spectra, while the complete series of experimental data is reported in Figure S5).

As expected, the CH_4 productivity increases upon increasing the temperature during CO_2 hydrogenation (T.o.S. = 0–20 min), as can be seen from the comparison of the MS signal of CH_4 in Figs. 6(a) and 5(a). Focusing on the species adsorbed on the catalyst surface (spectrum 1 in Fig. 6(b)), the amounts of carbonyls and formates decrease at this temperature with respect the experiment carried out at lower temperature. Switching to $H_2/CO/CO_2$ gas feed (T.o.S. = 30–50 min), the catalyst shows stable performance and, moreover, the amount of methane produced increases with respect to the pure CO_2 hydrogenation. The IR spectrum collected at the end of CO/CO_2 co-feeding period (spectrum 2 in Fig. 6(b)) shows that the bands related to CO are only slightly increased in the presence of CO. This behavior is due to the twofold effect of temperature, i.e. reduction of CO coverage and increase of the rate of adsorbed CO hydrogenation. Furthermore, no CH_x and carboxylate species are observed on the catalyst surface at 250 °C. After switching back to pure CO_2 hydrogenation (T.o.S. = 60–80 min) both the gas phase composition and the surface species are the same observed for the fresh catalyst (compare spectrum 1 and 3 in Fig. 6(b)).

These results are in agreement with the reactivity data collected in the fixed bed reactor for the Ru-SA catalyst (Figure S3(b)), although the process conditions were somewhat different. In fact, also in this case operating at high temperature reduces deactivation of Ru-based catalysts during CO/CO_2 methanation.

Fig. 7 sketches the state of the catalyst surface during the CO/CO_2 methanation, also schematically represented below (upper part: low-T; bottom part: high-T)

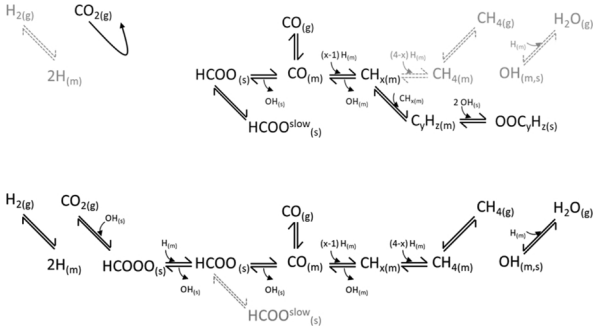

At low temperature CO is strongly adsorbed on the Ru sites, and this inhibits both CO_2 and H_2 adsorption, this latter limiting the methanation reaction. Due to the poor hydrogenating capability, carbonaceous C_yH_z groups and carboxylate species are produced on the catalyst surface and this progressively blocks the catalyst activity. Hence carboxylates and carbonaceous groups are blamed for catalyst deactivation,

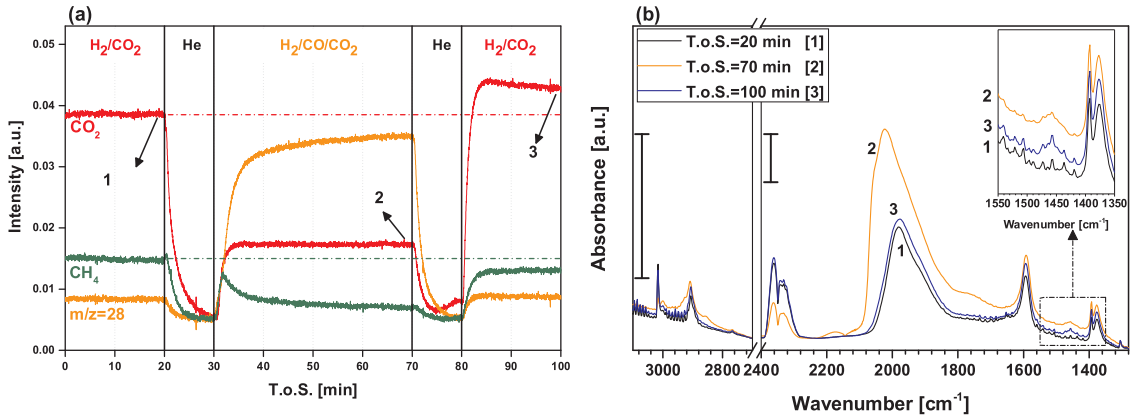

Fig. 5. (a) MS signals and (b) DRIFT spectra collected during the CO_x methanation at T = 200 °C. [Process conditions: P = 1 ata, F = 15 mL/min, H_2/CO_2/He = 8/2/90 (cond. 1, 3), $H_2/CO/CO_2$/He = 8/1.6/0.4/90 (cond. 2), catalyst: Ru-N].

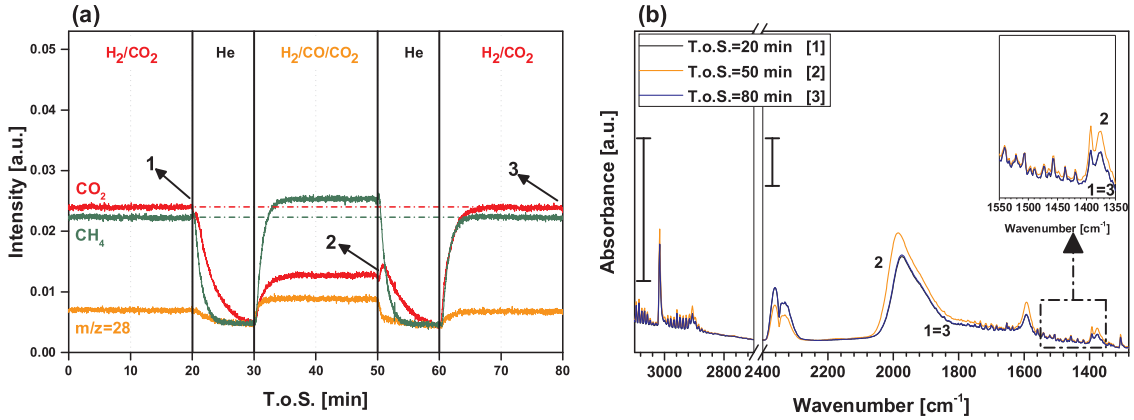

Fig. 6. (a) MS signals and (b) DRIFT spectra collected during the CO_x methanation at T = 250 °C. [Process conditions: P = 1 ata, F = 15 mL/min, H_2/CO_2/He = 8/2/90 (cond. 1, 3), $H_2/CO/CO_2$/He = 8/1.6/0.4/90 (cond. 2), catalyst: Ru-N].

along with the blockage of hydrogenation activity due to the strong CO adsorption on the metal sites.

At variance, working at high temperature reduces the amounts of adsorbed CO on Ru and hence increases the hydrogenating capability of the catalyst. No carboxylates and carbonaceous species are observed: very likely, the high hydrogenation activity at high temperature keeps the catalyst surface clean, allowing the CO_x methanation pathways to occur.

3.4. Reactivity of the adsorbed surface species

To better clarify the picture, the reactivity of the adsorbed species formed during the CO_x hydrogenation at 200 °C was investigated in the presence of H_2 at the same temperature. The catalyst surface after pure CO hydrogenation was chosen as starting point because all the important adsorbed species were present. IR spectra collected during this hydrogenation are reported in Fig. 8(a), while in Fig. 8(b) the decay of integrated intensities of the bands of adsorbed species is plotted in a log scale.

As apparent from Fig. 8, the most reactive species are the methylene groups, as the intensity of their characteristic band intensity quickly decays and disappear after about 5 min under H_2. The high reactivity of these species confirms their location on the Ru sites rather than on the Al_2O_3 support [46,79]. Furthermore, considering that these species are highly reactive with H_2, the increase of their concentration that is observed during the CO and CO/CO_2 methanation indicates the shortage

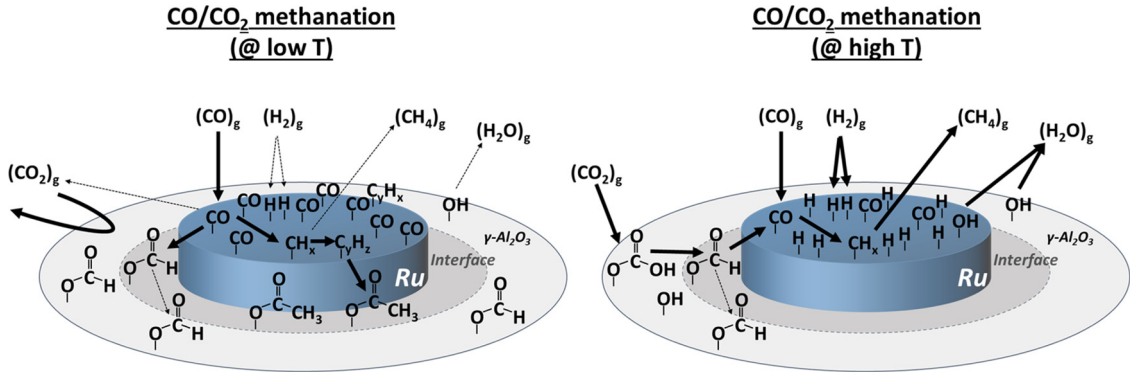

Fig. 7. Schematic rapresentation of the catalyst surface during CO/CO_2 methanation (solid arrows show main paths).

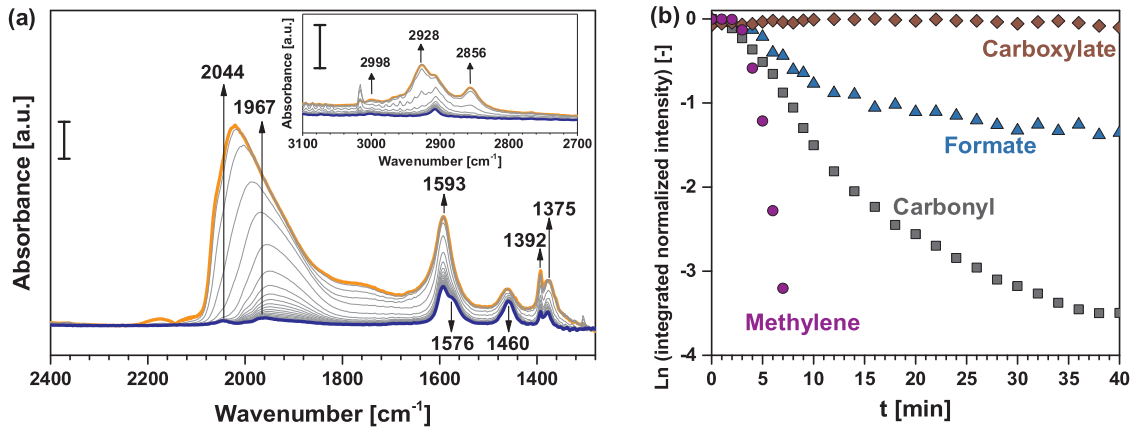

Fig. 8. (a) DRIFT spectra collected during a 40 min long hydrogenation treatment carried out after 8 h on stream of H_2/CO at T = 200 °C. (b) The natural logarithm decay for the adsorbed species during the hydrogenation step. [Process conditions: T = 200 °C, P = 1 ata, F = 15 mL/min, H_2/CO/He = 8/2/90 or H_2/ He = 8/92 M ratios, catalyst: Ru-N].

of active hydrogen on the ruthenium surface under the process conditions applied in this study. In fact, the only product detected by the MS is methane, meaning that adsorbed CH_x fragments are easily hydrogenated to methane.

Also the carbonyl band intensity almost completely disappears during the hydrogenation treatment, although with a slower rate. Looking at the temporal evolution of the IR features of adsorbed CO (Fig. 8(a)), a shift of the maximum from 2022 cm^{-1} to 1951 cm^{-1} can be observed, due to the decrease in the CO coverage. New features become also visible in the adsorbed CO band, and in particular two peaks become detectable at 2044 and 1967 cm^{-1}, related to geminal dicarbonyls adsorbed on low coordination Ru sites, where the hydrogenation is less favored [58]. The presence of these stable carbonyl species justifies the trend for the overall CO species intensity observed in Fig. 8(b), which does not follow a complete straight logarithmic decay, indicating that reactivity of carbonyl species is not uniform. The presence of these less reactive and highly stable species may be considered an additional cause of deactivation. Eventually, a CO supply contribution, coming from the formate hydrogenation and delaying carbonyl decay, has to be considered.

The decay curve of the formate species shows two distinct slopes: up to 10 min the slope is steep (high kinetic rate constant), followed by a slower process after about 10 min. As already reported in the literature for both CO_2 [57,58] and CO [81] methanation, this suggests that two types of formates are present. They are commonly classified as “fast” and “slow” formates, depending on their distance from the Ru particles. Formates close to the Ru particles (source of active hydrogen) react faster than those far away from the metal particles. It is worth noticing that the trends of formate and carbonyl intensities are similar, in that both show a change in the decay slope. This behavior supports the correlation existing between these species, where formates are intermediates of carbonyl formation when CO is not fed into the reactor (i.e. during CO_2 methanation).

Finally, the trend of the carboxylate species differs from that of all other species, since it does not show any decay during the H_2 treatment at 200 °C. As a result, the peak at 1576 cm^{-1}, associated with the asymmetric OCO-stretching of carboxylates, becomes visible due to the gradual disappearance of the 1593 cm^{-1} peak associated with the formates. Notably, the very different behaviors of the OCO-carboxylate vibrations and the methylene peaks indicates that these two fragments are unlikely related.

The reactivity of adsorbed species was additionally analyzed by carrying out experiments with a H_2/CO_2 = 1 feed stream, in order to slow down the evolution of the adsorbed species. In fact, in this way the bicarbonate species can be used as probe to check surface coverages on the alumina support, being this species certainly located on alumina [34,65–68]. Accordingly, experiments were carried out at 200 °C (i) on the fresh catalyst and (ii) on the catalyst that was previously deactivated in H_2/CO gas mixture for 24 h. IR spectra collected in these cases after 1 min and 40 min (black and red spectra, respectively) during the H_2/CO_2 reaction are presented in Fig. 9(a). The figure also shows the spectra obtained in the case of a “regenerated” sample, which will be discussed later on.

In the case of the fresh sample (case i), after 1 min on stream in H_2/CO_2 = 1 (black spectrum in Fig. 9(a)), the IR features of bicarbonates adsorbed on the alumina surface are significantly higher than those observed in the case of the H_2/CO_2 = 4 flow (Fig. 3(b)). However, after 40 min on stream (red spectrum), the surface species formed are similar to those observed with the H_2/CO_2 = 4 gas feed.

After the extensively deactivating treatment (case ii), methane formation during CO_2 hydrogenation is much lower, as confirmed by the intensity of the $\nu_{C\text{-}H}$ vibration of gas phase CH_4 at 3016 cm^{-1} (Fig. 9(a)). IR features of hydrocarbon, formate, carboxylate and carbonyl species are clearly seen, however no bicarbonates are detectable, not after 1 min on stream (black spectrum). This indicates that a portion of the alumina surface is blocked. After 40 min in the H_2/CO_2 gas mixture (red spectrum), the presence of hydrocarbons on the catalyst is still evident, although their intensities are effectively reduced, indicating a hydrogenation of these species during CO_2 methanation. Most importantly, no change occurs in the IR intensity of carboxylate feature, while that of the formates decreases with T.o.S. indicating their participation in the methanation reaction. All these results suggest that carboxylates block alumina sites participating in the CO_2 reduction by preventing the formation of bicarbonates. Besides, inspection of the IR spectra reveals that the shape of the carbonyl peak is slightly different during CO_2 hydrogenation over the fresh and the deactivated sample, as a shoulder is present near 1975 cm^{-1} in the case of the deactivated sample (case ii). This is likely associated to the influence of other surface species (i.e., carboxylates and/or hydrocarbons) in the proximity of Ru sites, which modifies the adsorption strength of CO on the ruthenium particles [82].

With the aim of recovering the catalyst reactivity, a regeneration treatment (heating under inert gas from 200 °C to 350 °C) was carried out. The IR spectra collected during this treatment are shown in Fig. 9(b) as a function of temperature, along with the intensity of the normalized integrated IR bands (Fig. 9(c)). The decomposition of formates (triangles) starts at 220 °C and their characteristic IR bands completely disappear at 310 °C. The onset temperature for the carboxylate decomposition is observed at higher temperatures, above 250 °C, indicating their higher thermal stability. The decay of the bands of adsorbed CO is somewhat peculiar, showing a two-step decrease with a steady level in the 250–350 °C temperature range. A comparison of this

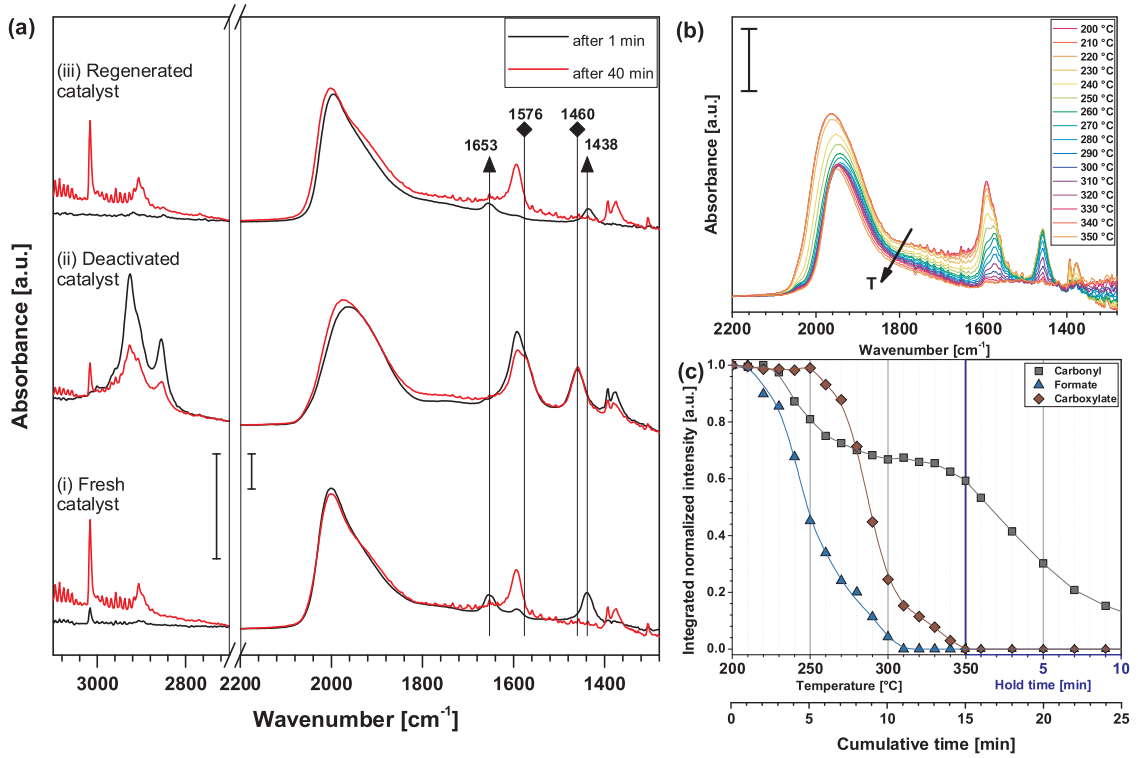

Fig. 9. (a) DRIFT spectra in the CO_2 hydrogenation on the catalyst previously treated: (i) fresh, (ii) deactivated by flowing H_2/CO/He = 8/2/90 for 24 h at 200 °C; (iii) regenerated by flowing pure He at 350 °C, heating ramp 10 °C/min and hold for 20 min. (b) DRIFT spectra and (c) adsorbed species intensity decay during the regeneration treatment. [Process conditions: T = 200 °C, P = 1 ata, F = 15 mL/min, H_2/CO_2/He = 5/5/90, catalyst: Ru-N].

trend with that of the carboxylate species suggests that the decomposition of carboxylates, characterized by a higher onset temperature, supplies CO to the Ru particles, and this leads to a decrease in the rate of the decrease of the carbonyl band. This may also indicate that carboxylate species are located near to the ruthenium sites, probably at the metal/support interface, differently from "slow formate" that are located far from the metal sites. This is in line with the reported carboxylate formation pathway assuming that hydrocarbons formed on the metal particles spill over to adsorption sites on alumina [74,75]. Carboxylates located in this position may also affect the peak shape of the adsorbed carbonyls as observed during CO_2 hydrogenation on the deactivated catalyst.

Eventually, the IR spectra were collected during CO_2 methanation over the regenerated catalyst (i.e. after heating under He flow) and results are shown in Fig. 9(a) (case iii). These spectra are very similar to those recorded in the case of the fresh sample; in particular the spectrum collected after 1 min in the H_2/CO_2 feed (black curve) clearly shows the presence of bicarbonates, indicating that the alumina surface is recovered during the high temperature regeneration in He, by decomposing and desorbing the carboxylate species.

The ability to totally recover the catalyst reactivity by increasing the temperature under inert gas flow was also confirmed by reactivity studies on both Ru-SA and Ru-N catalysts, as reported by Figure S6. These results point out that the temperature is the crucial parameter for catalyst regeneration, suggesting that activity recovery is mainly due to decomposition/desorption of C-containing species accumulated on the catalyst surface during CO methanation at low temperature. Furthermore, considering that catalytic activity can be completely recovered upon flowing an inert gas at high temperature, the deposition of carbon and/or formation of carbide on the catalyst surface (species not detectable with IR spectroscopy) seems to be unlikely the main reason of deactivation under the analyzed process conditions.

Eventually the spent Ru-N catalyst, deactivated by carrying CO methanation for 24 h, was analyzed by ex situ TEM imaging, after an in situ passivation step at room temperature by flowing 2 vol.% O_2 in N_2. The results, reported in Figure S2, show that the average size of Ru particles is only slightly increased after CO_x hydrogenation, although it is characterized by a more broadened size distribution than the fresh catalyst. However, since the catalyst activity is totally reversible, Ru sintering is excluded as main cause of deactivation.

4. Conclusion

In this work the reactivity of commercial and home-made Ru/Al_2O_3 catalysts in the CO/CO_2 methanation was investigated. Mechanistic aspects of the reaction were also investigated by DRIFTS experiments, and particular attention was paid on the reaction pathways and on the deactivation phenomena occurring when CO is present in the reacting mixture along with CO_2.

Both the catalysts are stable and highly selective in the CO_2 methanation. The presence of CO in the reacting CO_2/H_2 mixture at low temperatures leads to a decrease in the CO_2 conversion and, at high CO concentrations, a progressive deactivation of the catalyst. When switching the feed back to the CO-free atmosphere, a permanent deactivation is observed for high CO concentrations.

DRIFTS experiments, carried out over the home-made catalyst, show that the CO_2 hydrogenation reaction pathway is in line with that reported in the literature: carbon dioxide is adsorbed on the support as bicarbonate and is progressively hydrogenated to methane passing through the formation of formate adsorbed at the metal-support interface, and of carbonyl species on the metallic ruthenium surface.

When CO is present in the gas feed, the reaction sites for CO_2 hydrogenation are blocked by CO and the catalysts show deactivation, when operated at low temperature. The extent of activity loss increases upon increasing the CO/CO_2 ratio in the inlet gas stream and upon decreasing the catalyst temperature, thus suggesting a CO self-inhibition mechanism.

DRIFTS experiments confirm that, in the presence of gas phase CO

in the feed, the CO coverage is higher on the catalyst surface than that during methanation in pure CO_2. At high CO coverages, both the CO and CO_2 methanation reactions become kinetically inhibited due to the decrease of hydrogen concentration on the metal sites. Besides formates, carboxylates and carbonaceous species are formed and stay adsorbed on the catalyst surface. These species exhibit different reactivity, with carboxylates showing the highest stability. Indeed while hydrocarbons and formates can be removed by hydrogenation, carboxylates are very stable and cannot be removed. These stable oxide-bound surface species block adsorption sites for CO_2, thus lowering the CO_2 methanation activity of the catalyst even after the removal of CO from the gas feed stream. The observed deactivation, however, is reversible. By increasing the process temperature, even in inert gas flow, the catalyst activity can be completely recovered, due primarily to the thermal decomposition of the carboxylate species.

In conclusion, methanation in CO/CO_2 co-feed can be effectively carried out on Ru-based catalysts by working at temperatures high enough to prevent high CO coverage and the formation of stable carboxylate species, whose presence is the reason for catalyst deactivation.

Acknowledgments

Catalyst preparation, characterization and testing activity were carried out with a joint project between the Politecnico di Milano and the Italian National Agency for New Technologies, Energy and Sustainable Economic Development (ENEA), which is gratefully acknowledged. The authors gratefully acknowledge the financial support of the DRIFTS experiments by the US Department of Energy (DOE), Office of Science, Office of Basic Energy Sciences, Chemical Sciences, Geosciences, and Biosciences Division. L.F. also acknowledges the Pacific Northwest National Laboratory (PNNL) for the financial support during his stay as a visiting student.

Appendix A. Supplementary data

Supplementary material related to this article can be found, in the online version, at doi:https://doi.org/10.1016/j.apcatb.2019.117791.

References

[1] K.M.K. Yu, I. Curcic, J. Gabriel, S.C.E. Tsang, Recent advances in CO_2 capture and utilization, ChemSusChem 1 (2008) 893–899, https://doi.org/10.1002/cssc.200800169.
[2] M. Aresta, A. Dibenedetto, A. Angelini, Catalysis for the valorization of exhaust carbon: from CO_2 to chemicals, materials, and fuels. technological use of CO_2, Chem. Rev. 114 (2014) 1709–1742, https://doi.org/10.1021/cr4002758.
[3] B. Kumar, J.P. Brian, V. Atla, S. Kumari, K.A. Bertram, R.T. White, et al., New trends in the development of heterogeneous catalysts for electrochemical CO_2 reduction, Catal. Today 270 (2016) 19–30, https://doi.org/10.1016/j.cattod.2016.02.006.
[4] W. Wang, S. Wang, X. Ma, J. Gong, Recent advances in catalytic hydrogenation of carbon dioxide, Chem. Soc. Rev. 40 (2011) 3703–3727, https://doi.org/10.1039/c1cs15008a.
[5] K. Li, X. An, K. Hyeon, M. Khraisheh, J. Tang, A critical review of CO_2 photoconversion: catalysts and reactors, Catal. Today 224 (2014) 3–12, https://doi.org/10.1016/j.cattod.2013.12.006.
[6] IEA, Energy Technology Perspectives 2017 - Catalysing Energy Technology Transformations, (2016) www.iea.org/etp2017.
[7] IPCC, Climate Change 2014: Synthesis Report, Geneva, Switzerland, (2014), https://doi.org/10.1017/CBO9781107415324.
[8] V. Barbarossa, C. Bassano, P. Deiana, G. Vanga, CO_2 Conversion to CH_4, in: M. de Falco, G. Iaquaniello, G. Centi (Eds.), CO_2 A Valuab. Source Carbon, Springer-Verlag, 2013, pp. 123–145, , https://doi.org/10.1007/978-1-4471-5119-7.
[9] J. Gao, Q. Liu, F. Gu, B. Liu, Z. Zhong, F. Su, Recent advances in methanation catalysts for the production of synthetic natural gas, RSC Adv. 5 (2015) 22759–22776, https://doi.org/10.1039/C4RA16114A.
[10] M.A.A. Aziz, A.A. Jalil, S. Triwahyono, A. Ahmad, CO_2 Methanation over heterogeneous catalysts: recent progress and future prospects, Green Chem. 17 (2015) 2647–2663, https://doi.org/10.1039/C5GC00119F.
[11] M. Bailera, P. Lisbona, L.M. Romeo, S. Espatolero, Power to gas projects review: lab, pilot and demo plants for storing renewable energy and CO_2, Renew. Sustain. Energy Rev. 69 (2017) 292–312, https://doi.org/10.1016/j.rser.2016.11.130.
[12] S. Rönsch, J. Schneider, S. Matthischke, M. Schlüter, M. Götz, J. Lefebvre, et al., Review on methanation - from fundamentals to current projects, Fuel 166 (2016) 276–296, https://doi.org/10.1016/j.fuel.2015.10.111.
[13] M. Götz, J. Lefebvre, F. Mörs, A. McDaniel Koch, F. Graf, S. Bajohr, et al., Renewable power-to-gas: a technological and economic review, Renew. Energy 85 (2016) 1371–1390, https://doi.org/10.1016/j.renene.2015.07.066.
[14] F.D. Meylan, V. Moreau, S. Erkman, Material constraints related to storage of future European renewable electricity surpluses with CO_2 methanation, Energy Policy 94 (2016) 366–376, https://doi.org/10.1016/j.enpol.2016.04.012.
[15] T. Schaaf, J. Grünig, M.R. Schuster, T. Rothenfluh, A. Orth, Methanation of CO_2-storage of renewable energy in a gas distribution system, Energy. Sustain. Soc. 4 (2014) 1–14, https://doi.org/10.1186/s13705-014-0029-1.
[16] P. Sabatier, J.B. Senderens, Nouvelle synthèse du méthane, C. R. Acad. Sci. Paris 134 (1902) 514–516.
[17] J. Kopyscinski, T.J. Schildhauer, S.M.A. Biollaz, Production of synthetic natural gas (SNG) from coal and dry biomass - a technology review from 1950 to 2009, Fuel 89 (2010) 1763–1783, https://doi.org/10.1016/j.fuel.2010.01.027.
[18] T.A. Napp, A. Gambhir, T.P. Hills, N. Florin, P.S. Fennell, A review of the technologies, economics and policy instruments for decarbonising energy-intensive manufacturing industries, Renew. Sustain. Energy Rev. 30 (2014) 616–640, https://doi.org/10.1016/j.rser.2013.10.036.
[19] G.A. Mills, F.W. Steffgen, Catalytic methanation, Catal. Rev. Sci. Eng. 8 (1974) 159–210, https://doi.org/10.1080/01614947408071860.
[20] I. Czekaj, F. Loviat, F. Raimondi, J. Wambach, S. Biollaz, A. Wokaun, Characterization of surface processes at the Ni-based catalyst during the methanation of biomass-derived synthesis gas: X-ray photoelectron spectroscopy (XPS), Appl. Catal. A Gen. 329 (2007) 68–78, https://doi.org/10.1016/j.apcata.2007.06.027.
[21] C. Mirodatos, H. Praliaud, M. Primet, Deactivation of nickel-based catalysts during CO methanation and disproportionation, J. Catal. 107 (1987) 275–287, https://doi.org/10.1016/0021-9517(87)90294-6.
[22] M. Agnelli, M. Kolb, C. Nicot, C. Mirodatos, Sintering of a Ni-based catalyst during CO hydrogenation: kinetics and modeling, in: C.H. Bartholomew, J.B. Butt (Eds.), Catal. Deactiv. Elsevier B.V, Amsterdam, 1991, pp. 605–612.
[23] B. Miao, S.S.K. Ma, X. Wang, H. Su, S.H. Chan, Catalysis mechanisms of CO_2 and CO methanation, Catal. Sci. Technol. 6 (2016) 4048–4058, https://doi.org/10.1039/C6CY00478D.
[24] J.G. McCarty, H. Wise, Hydrogenation of surface carbon on alumina-supported nickel, J. Catal. 57 (1979) 406–416, https://doi.org/10.1016/0021-9517(79)90007-1.
[25] S. Helveg, C. López-Cartes, J. Sehested, P.L. Hansen, B.S. Clausen, J.R. Rostrup-Nielsen, et al., Atomic-scale imaging of carbon nanofibre growth, Nature 427 (2004) 5–8, https://doi.org/10.1038/nature02308.1.
[26] R.B. Anderson, The Fischer Tropsch Synthesis, Academic Press, Orlando, 1984.
[27] C. Janke, M.S. Duyar, M. Hoskins, R.J. Farrauto, Catalytic and adsorption studies for the hydrogenation of CO_2 to methane, Appl. Catal. B Environ. 152–153 (2014) 184–191, https://doi.org/10.1016/j.apcatb.2014.01.016.
[28] J.H. Kwak, L. Kovarik, J. Szanyi, CO_2 Reduction on supported Ru/Al_2O_3 catalysts: cluster size dependence of product selectivity, ACS Catal. 3 (2013) 2449–2455, https://doi.org/10.1021/cs400381f.
[29] M. Marwood, R. Doepper, M. Prairie, A. Renken, Transient drift spectroscopy for the determination of the surface-reaction kinetics of CO_2 methanation, Chem. Eng. Sci. 49 (1994) 4801–4809, https://doi.org/10.1016/S0009-2509(05)80060-0.
[30] P. Panagiotopoulou, D.I. Kondarides, X.E. Verykios, Mechanistic study of the selective methanation of CO over Ru/TiO_2 catalyst: effect of metal crystallite size on the nature of active surface species and reaction pathways, J. Phys. Chem. C 121 (2017) 5058–5068, https://doi.org/10.1021/acs.jpcc.6b12091.
[31] S. Sharma, Z. Hu, P. Zhang, E.W. McFarland, H. Metiu, CO_2 methanation on Ru-doped ceria, J. Catal. 278 (2011) 297–309, https://doi.org/10.1016/j.jcat.2010.12.015.
[32] D.C. Upham, A.R. Derk, S. Sharma, H. Metiu, E.W. McFarland, CO_2 methanation by Ru-doped ceria: the role of the oxidation state of the surface, Catal. Sci. Technol. 5 (2015) 1783–1791, https://doi.org/10.1039/C4CY01106F.
[33] L. Falbo, M. Martinelli, C.G. Visconti, L. Lietti, C. Bassano, P. Deiana, Kinetics of CO_2 methanation on a Ru-based catalyst at process conditions relevant for Power-to-Gas applications, Appl. Catal. B Environ. 225 (2018) 354–363, https://doi.org/10.1016/j.apcatb.2017.11.066.
[34] G. Garbarino, D. Bellotti, E. Finocchio, L. Magistri, G. Busca, Methanation of carbon dioxide on Ru/Al_2O_3: catalytic activity and infrared study, Catal. Today 277 (2016) 21–28, https://doi.org/10.1016/j.cattod.2015.12.010.
[35] A. Porta, L. Falbo, C.G. Visconti, L. Lietti, C. Bassano, P. Deiana, Synthesis of Ru-based catalysts for CO2 methanation and experimental assessment of intraporous transport limitations, Catal. Today (2019), https://doi.org/10.1016/j.cattod.2019.01.042.
[36] R. Mutschler, E. Moioli, W. Luo, N. Gallandat, A. Züttel, CO_2 hydrogenation reaction over pristine Fe, Co, Ni, Cu and Al_2O_3supported Ru: Comparison and determination of the activation energies, J. Catal. 366 (2018) 139–149, https://doi.org/10.1016/j.jcat.2018.08.002.
[37] F.S. Karn, J.F. Shultz, R.B. Anderson, Hydrogenation of carbon monoxide and carbon dioxide on supported ruthenium catalysts at moderate pressures, Ind. Eng. Chem. Prod. Res. Dev. 4 (1965) 265–269, https://doi.org/10.1021/i360016a014.
[38] J.M.G. Carballo, E. Finocchio, S. García-Rodriguez, M. Ojeda, J.L.G. Fierro, G. Busca, et al., Insights into the deactivation and reactivation of Ru/TiO_2 during Fischer-Tropsch synthesis, Catal. Today 214 (2013) 2–11, https://doi.org/10.1016/j.cattod.2012.09.018.
[39] C.H. Bartholomew, Mechanisms of catalyst deactivation, Appl. Catal. A Gen. 212 (2001) 17–60, https://doi.org/10.1016/S0926-860X(00)00843-7.
[40] H. Abrevaya, M.J. Cohn, W.M. Targos, H.J. Robota, Structure sensitive reactions

over supported ruthenium catalysts during Fischer-Tropsch synthesis, Catal. Lett. 7 (1990) 183–195, https://doi.org/10.1007/BF00764501.
[41] J.G. Goodwin, D.O. Goa, S. Erdal, F.H. Rogan, Reactive metal volatilization from Ru/Al_2O_3 as a result of ruthenium carbonyl formation, Appl. Catal. 24 (1986) 199–209, https://doi.org/10.1016/S0166-9834(00)81268-3.
[42] Tavlarides Mukkavilli, Tavlarides Wittmann, Carbon deactivation of Fischer-Tropsch ruthenium catalyst, Ind. Eng. Chem. Process Des. Dev. 25 (1983) 45, https://doi.org/10.1021/i200033a023.
[43] R.A. Dalla Betta, A.G. Piken, M. Shelef, Heterogeneous methanation: steady-state rate of CO hydrogenation on supported ruthenium, nickel and rhenium, J. Catal. 40 (1975) 173–183.
[44] R.M. Bowman, C.H. Bartholomew, Deactivation by carbon of Ru/Al_2O_3 during CO hydrogenation, Appl. Catal. 7 (1983) 179–187.
[45] R.A. Dalla Betta, M. Shelef, Heterogeneous methanation: in situ infrared spectroscopic study of Ru/Al_2O_3 during the hydrogenation of CO, J. Catal. 48 (1977) 111–119, https://doi.org/10.1016/0021-9517(77)90082-3.
[46] J.G. Ekerdt, A.T. Bell, Synthesis of hydrocarbons from CO and H_2 over silica-supported Ru: reaction rate measurements and infrared spectra of adsorbed species, J. Catal. 58 (1979) 170–187, https://doi.org/10.1016/0021-9517(79)90255-0.
[47] B.T. Loveless, C. Buda, M. Neurock, E. Iglesia, CO chemisorption and dissociation at high coverages during CO hydrogenation on Ru catalysts, J. Am. Chem. Soc. 135 (2013) 6107–6121, https://doi.org/10.1021/ja311848e.
[48] X. Wang, H. Shi, J. Szanyi, Controlling selectivities in CO_2 reduction through mechanistic understanding, Nat. Commun. 8 (2017) 1–6, https://doi.org/10.1038/s41467-017-00558-9.
[49] D.L. King, An in situ infrared study of CO hydrogenation over silica and alumina-supported ruthenium and silica-supported iron, J. Catal. 61 (1980) 77–86.
[50] N.W. Cant, A.T. Bell, Studies of carbon monoxide hydrogenation over ruthenium using transient response techniques, J. Catal. 73 (1982) 257–271, https://doi.org/10.1016/0021-9517(82)90099-9.
[51] P. Panagiotopoulou, D.I. Kondarides, X.E. Verykios, Mechanistic study of the selective methanation of CO over Ru/TiO_2 catalyst: identification of active surface species and reaction pathways, J. Phys. Chem. C 115 (2011) 1220–1230, https://doi.org/10.1021/jp106538z.
[52] O.R. Inderwildi, S.J. Jenkins, D.A. King, Mechanistic studies of hydrocarbon combustion and synthesis on noble metals, Angew. Chem. Int. Ed. 47 (2008) 5253–5255, https://doi.org/10.1002/anie.200800685.
[53] S. Eckle, H.G. Anfang, R.J. Behm, Reaction intermediates and side products in the methanation of CO and CO_2 over supported Ru catalysts in H_2-Rich reformate gases, J. Phys. Chem. C 115 (2011) 1361–1367, https://doi.org/10.1021/jp108106t.
[54] E. Zağli, J.L. Falconer, Carbon dioxide adsorption and methanation on ruthenium, J. Catal. 69 (1981) 1–8, https://doi.org/10.1016/0021-9517(81)90122-6.
[55] G.D. Weatherbee, C.H. Bartholomew, Hydrogenation of CO_2on Group VIII Metals II. Kinetics and Mechanism of CO_2 hydrogenation on Nickel, J. Catal. 77 (1982) 460–472.
[56] N.M. Gupta, V.S. Kamble, R.M. Iyer, K. Ravindranathan Thampi, M. Grätzel, The transient species formed over $Ru\text{-}RuO_x/TiO_2$ catalyst in the CO and CO + H_2 interaction : FTIR spectroscopic study, J. Catal. 137 (1992) 473–486.
[57] M. Marwood, R. Doepper, A. Renken, In-situ surface and gas phase analysis for kinetic studies under transient conditions the catalytic hydrogenation of CO_2, Appl. Catal. A Gen. 151 (1997) 223–246, https://doi.org/10.1016/S0926-860X(96)00267-0.
[58] X. Wang, Y. Hong, H. Shi, J. Szanyi, Kinetic modeling and transient DRIFTS-MS studies of CO_2 methanation over Ru/Al_2O_3 catalysts, J. Catal. 343 (2016) 185–195, https://doi.org/10.1016/j.jcat.2016.02.001.
[59] Y. Traa, J. Weitkamp, Kinetics of the Methanation of Carbon Dioxide over Ruthenium on Titania, Chem. Eng. Technol. 21 (1999) 291–293.
[60] J. Sirita, S. Phanichphant, F.C. Meunier, Quantitative analysis of adsorbate concentrations by diffuse reflectance FT-IR, Anal. Chem. 79 (2007) 3912–3918, https://doi.org/10.1021/ac0702802.
[61] H. Li, M. Rivallan, F. Thibault-Starzyk, A. Travert, F.C. Meunier, Effective bulk and surface temperatures of the catalyst bed of FT-IR cells used for in situ and operando studies, Phys. Chem. Chem. Phys. 15 (2013) 7321–7327, https://doi.org/10.1039/c3cp50442e.
[62] G.H. Yokomizo, A.T. Bell, Isotopic tracer and NMR studies of carbonaceous species present during CO hydrogenation over Ru TiO_2, J. Catal. 119 (1989) 467–482, https://doi.org/10.1016/0021-9517(89)90175-9.
[63] K.R. Krishna, A.T. Bell, An isotopic Tracer study of the deactivation of Ru/TiO_2 catalysts during Fischer-Tropsch synthesis, J. Catal. 130 (1991) 597–610.
[64] N.M. Gupta, V.P. Londhe, V.S. Kamble, Gas-uptake, methanation, and micro-calorimetric measurements on the coadsorption of CO and H_2 over polycrystalline Ru and a Ru/TiO_2 catalyst, J. Catal. 169 (1997) 423–437.
[65] J. Szanyi, J.H. Kwak, Dissecting the steps of CO_2 reduction: 1. The interaction of CO and CO_2 with γ-Al_2O_3: an in situ FTIR study, Phys. Chem. Chem. Phys. 16 (2014) 15117–15125, https://doi.org/10.1039/c4cp00616j.
[66] T. Montanari, L. Castoldi, L. Lietti, G. Busca, Basic catalysis and catalysis assisted by basicity: FT-IR and TPD characterization of potassium-doped alumina, Appl. Catal. A Gen. 400 (2011) 61–69, https://doi.org/10.1016/j.apcata.2011.04.016.
[67] C. Morterra, A. Zecchina, S. Coluccia, I.r. Spectroscopic Study of CO_2 adsorption onto η-Al_2O_2, J. Chem. Soc., Faraday Trans. 1 (73) (1977) 1544–11560, https://doi.org/10.1039/F19777301544.
[68] C. Morterra, G. Magnacca, A case study: surface chemistry and surface structure of catalytic aluminas, as studied by vibrational spectroscopy of adsorbed species, Catal. Today 27 (1996) 497–532, https://doi.org/10.1016/0920-5861(95)00163-8.
[69] G. Busca, J. Lamotte, J. Lavalley, V. Lorenzelli, FT-IR study of the adsorption and transformation of formaldehyde on oxide surfaces, J. Am. Chem. Soc. 109 (1987) 5197–5202, https://doi.org/10.1021/ja00251a025.
[70] R.A. Dalla Betta, Carbon monoxide adsorption on supported ruthenium, J. Phys. Chem. 79 (1975) 2519–2525, https://doi.org/10.1021/j100590a015.
[71] N.M. Gupta, V.S. Kamble, V.B. Kartha, R.M. Iyer, K. Ravindranathan Thampi, M. Grätzel, FTIR Spectroscopic Study of the Interaction of CO_2 and $CO_2 + H_2$ over Partially Oxidized Ru/TiO_2Catalyst, J. Catal. 146 (1994) 173–184, https://doi.org/10.1016/0021-9517(94)90020-5.
[72] S.Y. Chin, C.T. Williams, M.D. Amiridis, FTIR studies of CO adsorption on Al_2O_3- and SiO_2-supported Ru catalysts, J. Phys. Chem. B 110 (2006) 871–882, https://doi.org/10.1021/jp053908q.
[73] D. Lorito, A. Paredes-Nunez, C. Mirodatos, Y. Schuurman, F.C. Meunier, Determination of formate decomposition rates and relation to product formation during CO hydrogenation over supported cobalt, Catal. Today 259 (2015) 192–196, https://doi.org/10.1016/j.cattod.2015.06.027.
[74] J. Datka, Z. Sarbak, R.P. Eischens, Infrared study of coke on alumina and zeolite, J. Catal. 145 (1994) 544–550, https://doi.org/10.1006/jcat.1994.1065.
[75] Z. Sarbak, Fourier-transform infrared studies on coke formation over alumina silica-alumina and zeolites, React. Kinet. Catal. Lett. 69 (2000) 177–181.
[76] A. de Klerk, Fischer-Tropsch synthesis, Fischer-Tropsch Refin, Wiley-VCH Verlag GmbH & Co, KGaA, Weinheim, Germany, 2011, pp. 73–103, https://doi.org/10.1002/9783527635603.ch4.
[77] A.R. Garcia, J.L. da Silva, L.M. Ilharco, Chemical adsorption of acetic acid and deuterated acetic acid on Ru(0001), by RAIRS, Surf. Sci. 415 (1998) 183–193, https://doi.org/10.1016/S0039-6028(98)00590-1.
[78] P. Panagiotopoulou, D.I. Kondarides, X.E. Verykios, Mechanistic aspects of the selective methanation of CO over Ru/TiO_2 catalyst, Catal. Today 181 (2012) 138–147, https://doi.org/10.1016/j.cattod.2011.05.030.
[79] H. Yamasaki, Y. Kobori, S. Naito, T. Onishi, K. Tamaru, Infrared study of the reaction of $H_2 + CO$ on a Ru/SiO_2 catalyst, J. Chem. Soc. Faraday Trans. 1 Phys. Chem. Condens. Phases. 77 (1981) 2913–2925, https://doi.org/10.1039/F19817702913.
[80] J.A.H. Dreyer, P. Li, L. Zhang, G.K. Beh, R. Zhang, P.H.L. Sit, et al., Influence of the oxide support reducibility on the CO_2 methanation over Ru-based catalysts, Appl. Catal. B Environ. 219 (2017) 715–726, https://doi.org/10.1016/j.apcatb.2017.08.011.
[81] A. Paredes-Nunez, D. Lorito, N. Guilhaume, C. Mirodatos, Y. Schuurman, F.C. Meunier, Nature and reactivity of the surface species observed over a supported cobalt catalyst under CO/H_2 mixtures, Catal. Today 242 (2015) 178–183, https://doi.org/10.1016/j.cattod.2014.04.033.
[82] J.W. Niemantsverdriet, Spectroscopy in Catalysis: An Introduction, 3rd ed., WILEY-VCH Verlag GmbH & Co, KGaA, Weinheim, 2007, https://doi.org/10.1002/9783527611348.